

# Magnetic field measurements of sharp-lined Ap stars

S. P. Järvinen<sup>1\*</sup>, S. Hubrig<sup>1</sup>, R. Jayaraman<sup>2</sup>, I. Ilyin<sup>1</sup>, and M. Schöller<sup>3</sup>

<sup>1</sup>*Leibniz-Institut für Astrophysik Potsdam (AIP), An der Sternwarte 16, 14482 Potsdam, Germany*

<sup>2</sup>*MIT Kavli Institute and Department of Physics, 77 Massachusetts Avenue, Cambridge, MA 02139, USA*

<sup>3</sup>*European Southern Observatory, Karl-Schwarzschild-Str. 2, 85748 Garching, Germany*

Accepted 2022 August 19. Received 2022 August 18; in original form 2022 July 7

## ABSTRACT

Previous observations suggested that Ap and Bp stars exhibit a bimodal distribution of surface magnetic field strengths and that actually only few or no stars exist with magnetic dipole field strengths below 300 G down to a few Gauss. As the number of Ap and Bp stars currently known to possess weak magnetic fields is not large, it is necessary to carry out additional spectropolarimetric studies of Ap and Bp stars to prove whether the assumption of the existence of a critical value for the stability of magnetic fields is realistic. In this study, we present high-resolution HARPSpol magnetic field measurements for a sample of Ap stars with sharp spectral lines with a view to characterize the strengths of their magnetic fields. Out of the studied seven sharp-lined stars, two stars, HD 174779 and HD 203932, exhibit a rather weak longitudinal magnetic field with  $\langle B_z \rangle = -45 \pm 3$  G and  $\langle B_z \rangle = 21 \pm 4$  G, respectively. Additionally, TESS observations were used to test previous conclusions on the differentiation of rotation periods of Ap and Bp stars. Apart from HD 189832 and HD 203932, all other studied sharp-lined stars have long rotation periods. Since an explanation for the slow rotation of Ap stars is currently missing, additional studies of slowly rotating Ap and Bp stars are necessary to improve our understanding of the formation and evolution of Ap and Bp stars.

**Key words:** stars: chemically peculiar – stars: individual: HD 70702, HD 89393, HD 137949, HD 138633, HD 174779, HD 176196, HD 189832, HD 203932, HD 217522 – stars: magnetic fields – stars: rotation

## 1 INTRODUCTION

Large-scale organised magnetic fields with strengths ranging from several tens of Gauss to several kG are present in 10 to 15% of all stars of spectral types O to early F (e.g. Grunhut et al. 2017; Schöller et al. 2017; Hubrig & Schöller 2021). Magnetic fields cover the whole stellar surface, and their geometry often resembles a single dipole whose axis is inclined with respect to the stellar rotation axis. Understanding how these stars acquired magnetic fields and why they are only present in a fraction of upper main-sequence stars, as well as how these fields affect stellar evolution, will have significant implications for a wide range of astrophysical areas, from galactic evolution to exoplanets. Studies of upper main-sequence Ap and Bp stars, constituting the most populous group of magnetic early-type stars, are also of great importance because such stars display the most extreme manifestations of the effects of magnetic fields on stellar atmospheres. Specifically, they exhibit strong abundance anomalies, including both the horizontal accumulation and vertical stratification of abundances of various chemical elements.

Based on mean longitudinal magnetic field measurements (i.e. measurements of the line-intensity weighted average over the stellar disc of the component of the magnetic vector along

the line of sight) of a small sample of 28 magnetic Ap and Bp stars with poorly constrained magnetic field strengths, Aurière et al. (2007) concluded that there exists a critical dipole field strength,  $B_d \approx 300$  G, which corresponds to the minimum field strength for a star to maintain the stability of its magnetic field. Only two stars in the sample of 28 Ap stars showed a dipole strength below 300 G. The authors suggested that the magnetic dichotomy of intermediate-mass stars – i.e., a dichotomy in the distribution of the observed magnetic field between the kG dipoles of Ap and Bp stars and the sub-Gauss magnetism of Vega and Sirius – arise from the development of non-axisymmetric instabilities separating stable strong field configurations observed in Ap and Bp stars from unstable weaker field configurations, whose surface average field becomes very weak after the destabilization. However, in contrast to this study, a number of Ap and Bp stars have been reported to possess very weak longitudinal magnetic fields on the order of a few tens of Gauss (e.g., Donati, Semel & del Toro Iniesta 1990; Donati et al. 2006; Alecian et al. 2016). Also, for higher mass Bp stars, rather weak magnetic fields were reported by Fossati et al. (2015). As discussed by Jermyn & Cantiello (2020), such weak fields can be consistent with dynamo fields generated in subsurface convection zones. Since the reported dichotomy may be due to observational incompleteness, there is certainly a need for more representative studies of Ap and Bp stars. Such studies are especially

\* E-mail: sjarvinen@aip.de

important for the theoretical understanding of the origin of magnetic Ap and Bp stars.

The other important question for the understanding of the origin of magnetic Ap and Bp stars with sharp lines is whether the majority of stars with weak magnetic fields are slow rotators. If these stars are not observed close to the rotation pole, then we expect that a fraction of stars with very sharp spectral lines have longer rotation periods. The occurrence of very slow rotation in weakly magnetic Ap and Bp stars has not been investigated in detail yet, but is becoming an important subject of current studies of correlations between rotation rate and magnetic field strength, following the recent discovery of unbiased Transiting Exoplanet Survey Satellite (TESS; [Ricker et al. 2015](#)) samples of slowly rotating Ap stars by [Mathys, Kurtz & Holdsworth \(2020, 2022\)](#). According to [Hubrig, North & Schöller \(2007\)](#), stronger magnetic fields tend to be found in hotter, younger and more massive stars, as well as in stars with shorter rotation periods. [Mathys \(2017\)](#) confirmed that Ap stars with very strong magnetic fields never achieve extremely slow rotation: Ap stars with  $\langle B \rangle > 7.5$  kG have rotation periods shorter than 150 d whereas Ap stars with  $\langle B \rangle < 7.5$  kG have periods longer than 150 d. Thus, the differentiation of rotation in Ap and Bp stars is a possible key to the understanding of the origin of their magnetic fields.

In this work, we discuss new mean longitudinal magnetic field measurements for a sample of sharp-lined Ap stars using the High Accuracy Radial velocity Planet Searcher polarimeter, (HARPSpol; [Snik et al. 2008](#)) fed by the ESO 3.6-m telescope. In the spectra of several of the Ap and Bp stars obtained in the framework of a systematic search for Ap stars with resolved magnetically split lines, spectral lines appear very sharp. This indicates that magnetic line broadening, which is proportional to the absolute value of the magnetic field strength, should be very small. For a number of stars in our sample, photometric data have recently been provided by the TESS mission, enabling us to search for variability in their light curves. As the surfaces of Ap and Bp stars are covered by long-lived chemical spots that rotate in and out of view, the light curves show rotational modulation. Usually, the light curves exhibit different shapes and amplitudes, depending on the size of the spots and their location with respect to the line of sight. The availability of space-based photometric observations is especially valuable in studies of Ap and Bp stars, as their rotation periods are most frequently determined from light curves.

Among the stars in our sample, magnetic field measurements are carried out for the first time for the sharp-lined stars HD 89393, HD 174779, and HD 189832. In the spectra of HD 138633, HD 176196, HD 203932, and HD 217522, the spectral lines are also sharp and do not show any hint of resolution into their magnetic Zeeman components, but the possible presence of relatively weak magnetic fields was already discussed in previous studies. The very slowly rotating star HD 137949, which possesses a rather strong magnetic field and exhibits spectral lines resolved into magnetically split components, was previously reported to have a rotation period of more than 14 yr by [Mathys \(2017\)](#). However, their published magnetic field measurements for this star were taken in 1997. The strongly magnetic star HD 70702, with a magnetic field modulus of about 15 kG, was selected in our observations as a standard star to check the proper techni-

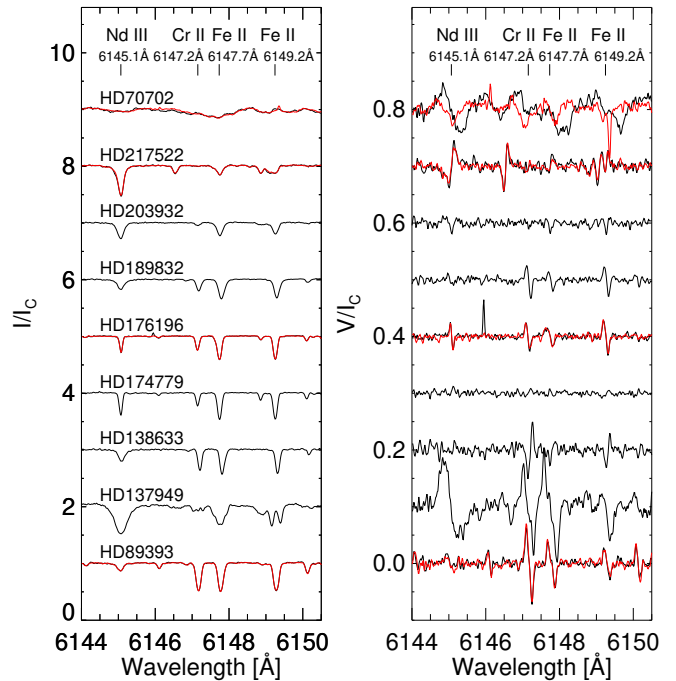


**Figure 1.** HARPSpol Stokes  $I$  (left side) and Stokes  $V$  (right side) spectra in the spectral region containing spectral lines characteristic for Ap stars. The spectra are overplotted for stars which were observed twice. The identified lines are Nd III at 6145.1 Å, Cr II at 6147.2 Å, Fe II at 6147.7 Å, and Fe II at 6149.2 Å. All spectra are shifted to the laboratory wavelengths for comparison reasons.

cal functionality of the analysing optics of HARPSpol during our observing run in 2019. Observations of this star at two different rotation phases indicate strong changes in the magnetic field strengths and variable spectral appearance. Strongly magnetic stars are of special interest because only in these stars the effect of the magnetic field on the stellar atmosphere can be studied in great detail. Since magnetism affects atomic diffusion (e.g. [Alecian & Stift 2019](#)), the obtained information on the magnetic field geometry is frequently used to study the horizontal accumulation and vertical stratification of abundances of various chemical elements (e.g. [Hubrig et al. 2018; Järvinen et al. 2020](#)).

In the following sections we present the acquired HARPSpol observations, their reduction and the analysis, describe the measurement results for each individual target, and discuss their usefulness for a better understanding of stellar magnetism in Ap and Bp stars. All available TESS data are also used to identify any significant periodicities.

## 2 OBSERVATIONS

### 2.1 HARPSpol observations

All spectropolarimetric observations used in our work were acquired with HARPSpol on the ESO 3.6-m telescope on La Silla, which has a resolving power of  $R = 115\,000$  and a wavelength coverage from 3780 to 6910 Å, with a small gap between 5259 and 5337 Å. Observations were carried out in 2019 June (Prg. ID 0103.C-0240). Additionally, we discuss

**Table 1.** The logbook of observations and the results of the magnetic field measurements for the investigated stars based on line lists that include all lines. The first column gives the name of the star followed by the spectral classification from [Renson & Manfroid \(2009\)](#). The third column presents the MJD values at the middle of the exposure, while the fourth column presents the signal to noise ratio measured in the spectral region shown in Fig. 1. The remaining columns show the total number of lines in each line mask, the average effective Landé factor  $\bar{g}_{\text{eff}}$  calculated for each line mask, the measured LSD mean longitudinal magnetic field strength, the false alarm probability (FAP) value for each measurement, and the detection flag, where DD means definite detection, MD marginal detection, and ND no detection.

Object	Spectral Type	MJD	$S/N$	N. of lines	$\bar{g}_{\text{eff}}$	$\langle B_z \rangle$ (G)	FAP	Det. flag
HD 89393	A0 SrCrEu	58 646.094	434	86	1.20	314±7	< 10 <sup>-10</sup>	DD
		58 649.023	351			321±6	< 10 <sup>-10</sup>	DD
HD 137949	F0 SrEuCr	56 145.020	175	173	1.18	1543±19	< 10 <sup>-10</sup>	DD
HD 138633	F0 SrEuCr	58 650.051	239	116	1.21	-205±9	< 10 <sup>-10</sup>	DD
HD 174779	A0 Si	58 647.316	324	80	1.21	-45±3	< 10 <sup>-10</sup>	DD
HD 176196	B9 EuCr	58 648.375	309	96	1.21	120±18	< 10 <sup>-10</sup>	DD
		58 650.344	402			109±17	< 10 <sup>-10</sup>	DD
HD 189832	A6 SrCrEu	58 647.406	311	141	1.22	143±4	< 10 <sup>-10</sup>	DD
HD 203932	A5 SrEu	58 648.430	290	141	1.20	21±4	< 10 <sup>-10</sup>	DD
HD 217522	A5 SrEuCr	56 148.297	218	120	1.24	-401±6	< 10 <sup>-10</sup>	DD
		58 647.438	363			-323±6	< 10 <sup>-10</sup>	DD
HD 70702	B9 EuCrSr	58 648.008	188	72	1.19	4388±169	< 10 <sup>-10</sup>	DD
		58 650.973	319			1233±102	< 10 <sup>-10</sup>	DD

archival observations for HD 137949 and HD 217522, which were obtained in 2012 August (Prg. ID 089.D-0383). The data reduction was carried out on La Silla using the HARPS data reduction pipeline. The normalization of the spectra to the continuum level is described in detail by [Hubrig et al. \(2013\)](#). More details on the observations are presented in Table 1. For each star in our sample, HARPSpol Stokes  $I$  and Stokes  $V$  spectra in the spectral region containing spectral lines characteristic for Ap stars are presented in Fig. 1.

## 2.2 UVES and CES

To check the short- and long-term line profile variability of HD 138633, we extracted from the ESO archive high-resolution observations obtained with UVES (the Ultraviolet and Visual Echelle Spectrograph) mounted on Unit Telescope 2 (UT2) of the Very Large Telescope (VLT) at Cerro Paranal, Chile (Prg. ID 072.D-013, carried out on 2004 March 5), as well as two observations with the CES Very Long Camera, which was previously installed at the 1.4 m CAT telescope (Prg. ID 68.D-0445, carried out on 2002 January 25). The original UVES data consist of a large amount of very short, noisy exposures covering the wavelength range 4959–7071 Å and a spectral resolution  $R = 107\,000$ . The individual UVES files were combined into one final spectrum with  $S/N = 456$  using the ESO Phase 3 UVES pipeline<sup>1</sup>. Wavelength calibrations for the CES spectra were executed by utilising the Th-Ar comparison spectra obtained immediately before and after recording the stellar spectrum. The first spectrum has an exposure time of 600 s, whereas the second spectrum was obtained 14 minutes later with an exposure time of 780 s.

## 2.3 TESS photometry

For three stars in our sample, HD 176196, HD 203932, and HD 217522, an analysis of TESS photometry was presented in the past. No variability was detected by [Mathys, Kurtz & Holdsworth \(2020\)](#) in the available TESS data for HD 176196 and HD 217522. Both stars were classified by these authors as super slowly rotating Ap (ssrAp) stars. [Cunha et al. \(2019\)](#) and [Holdsworth et al. \(2021\)](#) analysed TESS data for HD 203932 and reported a rotation period of  $6.44 \pm 0.01$  d, and pulsation periods of 2.6985 and 2.8048 mHz, confirming that this star is a rapidly oscillating Ap (roAp) star.

Three stars – HD 70702, HD 89393, and HD 174779 – were observed during Year 1 of the TESS mission, in sectors 8 and 9, sector 9, and sector 13, respectively<sup>2</sup>, but no analysis of the data for these stars has been reported in the past. In our study, the 2-minute cadence TESS observations in sectors 8–9 are used to search for periodicity in the light curve of HD 70702. HD 89393 has 2-min cadence data from sector 9 and 10-min full frame image (FFI) data from sector 36, while HD 174779 has 2-minute cadence data from sector 13. No TESS data exist for HD 137949, but it was observed as a part of the Kepler ([Borucki et al. 2009](#)) K2 ([Howell et al. 2014](#)) Campaign 15, from mid- to late-2017, in 1-minute cadence. In addition, we discuss the analysis of TESS data of HD 138633, which was observed in sector 51 in 2022 May. We do not have TESS data for HD 189832, which will be observed in sector 67, probably in 2023 July.

The shorter-cadence data from both Kepler and TESS are available in both simple aperture photometry (SAP) and pre-search data conditioning SAP (PDCSAP) forms. Data processing was done using the Science Processing Operations Center (SPOC) pipeline at the NASA Ames Research Center ([Jenkins et al. 2016](#)). With the PDCSAP light curves, we performed a Discrete Fourier Transform (DFT; see, e.g. [Kurtz](#)

<sup>1</sup> <http://www.eso.org/rm/api/v1/public/releaseDescriptions/163>

<sup>2</sup> These observations occurred between 2018 July to 2019 July.

1985) to identify the dominant frequency components of the signal and their amplitudes.

### 3 MAGNETIC FIELD MEASUREMENTS AND DETECTED PERIODICITIES

To increase the  $S/N$  in our polarimetric measurements, we employed the least-squares deconvolution (LSD) technique. The details of this technique, as well as how Stokes  $I$  and Stokes  $V$  parameters are calculated, were presented by Donati et al. (1997). The line masks were constructed using the Vienna Atomic Line Database (VALD3; Kupka et al. 2011). For each star, we carefully checked that the selected lines are indeed present in the Stokes  $I$  spectra and do not show severe blending. The presence of a magnetic field is evaluated following Donati, Semel, & Rees (1992), who defined that a Zeeman profile with a false alarm probability (FAP)  $\leq 10^{-5}$  is considered as a definite detection (DD),  $10^{-5} < \text{FAP} \leq 10^{-3}$  as a marginal detection (MD), and  $\text{FAP} > 10^{-3}$  as a non-detection (ND).

Previous studies of magnetic Ap and Bp stars showed that the lines of different elements with different abundance distributions across the stellar surface sample the magnetic field in different ways. Some elements, such as rare-earth elements (REEs), are frequently observed to concentrate close to the magnetic poles, whereas other elements cluster in regions closer to the magnetic equator. Combining lines of all elements together in the LSD line masks may lead to the dilution of the magnetic signal or even to its (partial) cancellation, if enhancements of different elements occur in regions of opposite magnetic polarities. Therefore, it is advisable to use in the measurements line masks constructed for individual elements. Among the REEs, Pr, Nd, and Eu are well known to be concentrated in surface spots, whereas Fe shows a rather uniform surface distribution. Using line masks constructed for Fe I, Fe II, Pr III, Nd III, and Eu II for the magnetic field measurements, it is possible to get information about the differences in the individual surface distributions of these ions. We note that we do not actually know the magnetic field geometries of the stars in our sample, but we should still be able to identify the locations of surface element spots if different field strengths are derived by the application of the LSD technique to different line masks.

The LSD longitudinal magnetic field  $\langle B_z \rangle$  measurements based on line masks that include the combined spectral lines belonging to different elements are listed in Table 1, and the corresponding LSD profiles are shown in Fig. 2. The results of the LSD magnetic field measurements for all stars using individual line masks with the spectral lines of Fe I, Fe II, Pr III, Nd III, and Eu II are presented in Table 2.

For each star, the results of our magnetic field measurements and the available information on the periodicities are discussed in the following subsections. When studying the stars' periodicities using TESS observations, we identified a frequency as significant if it has a signal-to-noise ratio  $S/N \geq 4.5$  and marginal if  $3 \leq S/N < 4.5$ . Any peaks with  $S/N < 3$  were discarded as being consistent with noise and therefore merited no further investigation.

#### 3.1 HD 89393

Not much is known about this star. It is classified as A0 SrCrEu in Renson & Manfroid (2009). Magnetic field measurements were not reported for this star in the past. In Fig. 3, we present the LSD Stokes  $I$ , Stokes  $V$ , and diagnostic null  $N$  profiles for this star, calculated using five different masks. The mean longitudinal field strengths obtained at both epochs are almost identical (see also Tables 1 and 2 and Fig. 2), indicating the absence of any short-timescale variability. The amplitude of the Zeeman features and the measured field values clearly depend on the line masks constructed for individual elements, as the strongest mean longitudinal magnetic field is detected in the measurements using the Eu II line mask, suggesting a slightly different location (probably closer to the magnetic pole) of the Eu concentration on the stellar surface in comparison to other elements.

The TESS light curve of HD 89383 is shown in the left panel of Fig. 4. The CROWDSAP parameter suggests that there is significant contamination from a nearby star (TYC 7712-2715-1). The CROWDSAP parameter refers to the fraction of flux that falls in the optimal aperture for the 2-minute data that is not directly attributable to the star in question (i.e. a ‘‘crowding parameter’’) and is calculated as part of the SPOC pipeline when data products are produced. The Gaia BP–RP colour index (Gaia Collaboration 2018) for this nearby contaminating star is greater than 1, suggesting that it is a cooler star. The periodogram shows just one marginal peak with a calculated  $S/N$  of  $\sim 4$  at a period of  $0.34116 \pm 0.00001$  d. Since our metric is the relative amplitude of the peaks in the periodograms, we do not attach any physical interpretation to this marginal peak and are not able to conclude whether this frequency could represent a pulsation mode or arises from some other physical phenomenon, such as rotation of either HD 89393 or the contaminating star. We assume that HD 89393 likely has a long rotation period; this must at least be longer than the length of the TESS observations over 27 d. Also the examination of the 10 min cadence TESS data in sector 36 did not reveal any significant peak in our periodogram.

#### 3.2 HD 137949 = 33 Lib

The star is classified as F0 SrEuCr in Renson & Manfroid (2009). It is a roAp star with a pulsation period of 8.3 min (Kurtz 1982). The study of Kervella et al. (2019) indicated the presence of a companion from an analysis of proper motions in the Gaia Data Release 2 (GDR2; Gaia Collaboration 2018) and Hipparcos (van Leeuwen 2007) catalogues. A strong mean longitudinal magnetic field with a value of more than 1 kG was initially discovered in this star by Babcock (1958). Given the presence of the strong magnetic field and the slow rotation, numerous spectral lines are resolved into their magnetically split components. The most complete review of the previous magnetic studies of 33 Lib is presented in Mathys (2017). Their seven measurements of the mean magnetic field modulus  $\langle B \rangle$  using magnetically resolved lines in observations acquired between 1996 and 1998 appear to be constant in the range from 4.63 to 4.69 kG, whereas the  $\langle B_z \rangle$ -values from the same observations range from 1.47 to 1.68 kG. Taking into account all previous measurements of



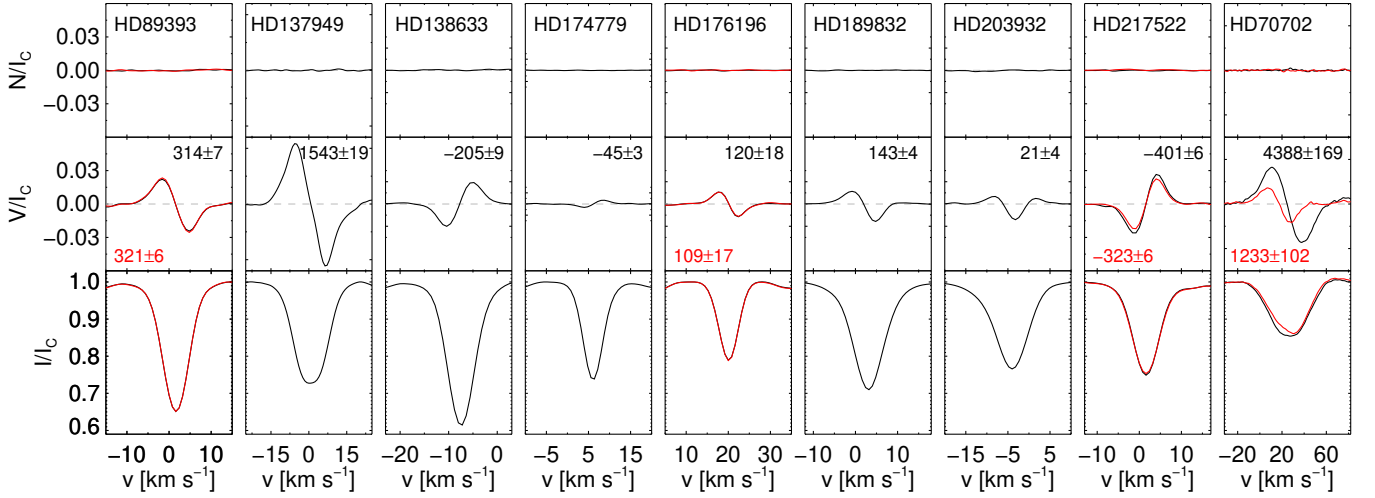


**Figure 2.** LSD Stokes  $I$ , Stokes  $V$ , and diagnostic null  $N$  profiles (from bottom to top) calculated for the investigated stars combining line masks that include spectral lines belonging to different ions (Fe I, Fe II, Pr III, Nd III, and Eu II). For stars with two observations, the profiles have been overlotted, and the profiles from the latter epoch are shown in red. In all plots we also present the measured mean longitudinal magnetic field strengths, colour-coded in the same way as the spectra.

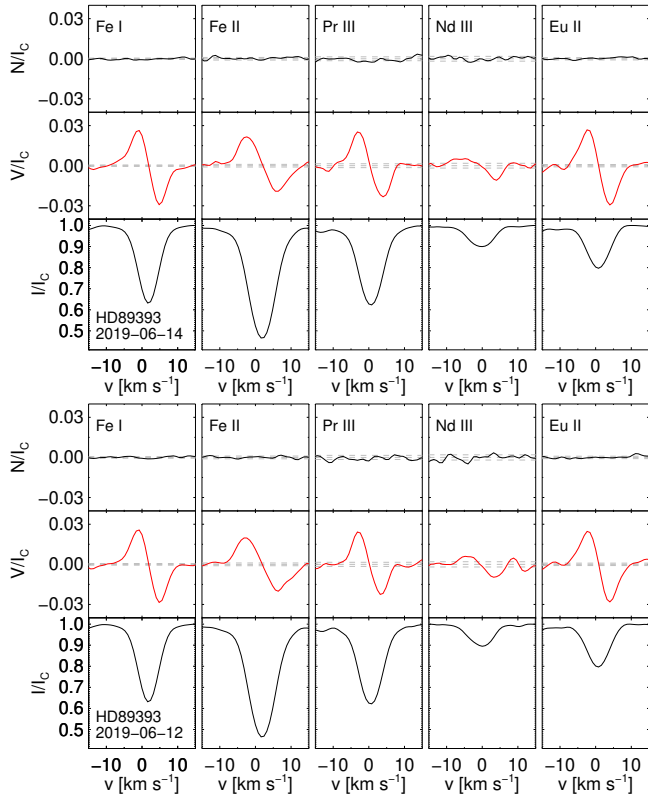


**Figure 3.** LSD Stokes  $I$ , Stokes  $V$ , and diagnostic null  $N$  profiles (from bottom to top) calculated for the two observing epochs of HD 89393 using line masks containing Fe I, Fe II, Pr III, Nd III, and Eu II lines (from left to right).

$\langle B_z \rangle$ -values, Mathys (2017) suggest that this star has a rotational period  $P_{\text{rot}}$  of 5195 d (approximately 14.25 yr).

On the other hand, Giarrusso et al. (2022) recently reported that  $\langle B \rangle$  and  $\langle B_z \rangle$ -values have shown a slight increase

over several years, indicating that the rotation period should be longer than 27 yr. Our measurement of the mean field modulus using the HARPSpol observations obtained in 2012 August,  $\langle B \rangle = 4.76 \pm 0.02$  kG, is of the same order as reported by Giarrusso et al. (2022). As an illustration, we show the Zeeman subcomponents of the resolved magnetically split Fe II line at 6149.258 Å in Fig. 5. No measurements of the mean longitudinal magnetic field after 2007 were presented by Giarrusso et al. (2022). Our measurement of the mean longitudinal field strength using all lines,  $\langle B_z \rangle = 1.54 \pm 0.02$  kG, does not confirm the slight increase, but the small differences in the field values can be caused by the choice of spectral lines used in the measurements. As we see in Fig. 6, which presents the LSD Stokes  $I$ , Stokes  $V$ , and diagnostic null  $N$  profiles calculated using five different masks, and in Table 2, the amplitude of the Zeeman features and the measured field values for this star depend on the line masks constructed for individual elements: We measure  $\langle B_z \rangle = 1.94 \pm 0.05$  kG using 34 Pr III lines, but only  $\langle B_z \rangle = 1.09 \pm 0.04$  kG using 14 Nd III lines. In any case, the comparison of our measurements with previous measurements confirm a long rotation period for HD 137949.

A full analysis of short-period oscillations (typical for roAp stars) was done for HD 137949 by Holdsworth et al. (2018) based on 60-s cadence K2 observations. The authors found that the low-frequency peaks were aliases of the frequency splitting, and that the rotation period was likely extremely long. The amplitude spectra of 33 Lib were presented in Figures 1 and 2 of Holdsworth et al. (2018).

### 3.3 HD 138633

This star is classified as F0SrEuCr in Renson & Manfroid (2009). The presence of a weak magnetic field of the order of 0.7 kG was announced by Titarenko et al. (2013). They report that in contrast to ordinary Ap stars that exhibit strong REE lines in their spectra, these elements are represented

**Table 2.** The LSD mean longitudinal magnetic field measurements for all targets using five different line masks are presented along with the MJD values, number of lines in each mask, the average Landé factors, and the FAP values. DD means definite detection, MD marginal detection, and ND no detection.

MJD	Mask	$\bar{g}_{\text{eff}}$	$\langle B_z \rangle$ (G)	FAP	Det. flag	MJD	Mask	$\bar{g}_{\text{eff}}$	$\langle B_z \rangle$ (G)	FAP	Det. flag
HD 89393						HD 189832					
58 646.094	Fe I (49)	1.16	343±9	< 10 <sup>-10</sup>	DD	58 647.406	Fe I (97)	1.22	151±4	< 10 <sup>-10</sup>	DD
	Fe II (14)	1.17	262±14	< 10 <sup>-10</sup>	DD		Fe II (17)	1.11	160±11	< 10 <sup>-10</sup>	DD
	Pr III (5)	1.11	246±20	< 10 <sup>-10</sup>	DD		Pr III (10)	0.96	184±21	< 10 <sup>-10</sup>	DD
	Nd III (6)	1.04	260±43	0.052	ND		Nd III (2)	1.09	166±35	0.081	ND
	Eu II (12)	1.54	436±20	< 10 <sup>-10</sup>	DD		Eu II (15)	1.50	84±20	1 × 10 <sup>-6</sup>	DD
58 649.023	Fe I (49)	1.16	349±10	< 10 <sup>-10</sup>	DD	HD 203932					
	Fe II (14)	1.17	240±16	< 10 <sup>-10</sup>	DD	58 648.430	Fe I (98)	1.21	3±5	< 10 <sup>-10</sup>	DD
	Pr III (5)	1.11	292±18	< 10 <sup>-10</sup>	DD		Fe II (10)	1.17	38±13	< 10 <sup>-10</sup>	DD
	Nd III (6)	1.04	249±39	0.026	ND		Pr III (8)	0.92	99±42	< 10 <sup>-10</sup>	DD
	Eu II (12)	1.54	461±17	< 10 <sup>-10</sup>	DD		Nd III (24)	1.19	37±15	< 10 <sup>-10</sup>	DD
					Eu II (5)		1.65	150±19	< 10 <sup>-10</sup>	DD	
HD 137949						HD 217522					
56 145.020	Fe I (98)	1.20	1548±32	< 10 <sup>-10</sup>	DD	56 148.297	Fe I (80)	1.23	-358±7	< 10 <sup>-10</sup>	DD
	Fe II (19)	1.16	1291±55	< 10 <sup>-10</sup>	DD		Fe II (9)	1.10	-429±36	< 10 <sup>-10</sup>	DD
	Pr III (34)	1.03	1941±48	< 10 <sup>-10</sup>	DD		Pr III (6)	1.07	-552±59	< 10 <sup>-10</sup>	DD
	Nd III (14)	1.24	1091±38	< 10 <sup>-10</sup>	DD		Nd III (20)	1.30	-343±6	< 10 <sup>-10</sup>	DD
	Eu II (8)	1.54	1368±30	< 10 <sup>-10</sup>	DD		Eu II (5)	1.60	-423±8	< 10 <sup>-10</sup>	DD
HD 138633						58 647.438	Fe I (80)	1.23	-264±7	< 10 <sup>-10</sup>	DD
58 650.051	Fe I (84)	1.21	-204±10	< 10 <sup>-10</sup>	DD		Fe II (9)	1.10	-345±30	< 10 <sup>-10</sup>	DD
	Fe II (11)	1.07	-160±27	< 10 <sup>-10</sup>	DD		Pr III (6)	1.07	-426±40	< 10 <sup>-10</sup>	DD
	Pr III (11)	1.07	-257±30	< 10 <sup>-10</sup>	DD		Nd III (20)	1.30	-309±6	< 10 <sup>-10</sup>	DD
	Nd III (4)	1.06	-174±26	7 × 10 <sup>-4</sup>	MD		Eu II (5)	1.60	-413±8	< 10 <sup>-10</sup>	DD
	Eu II (6)	1.75	-182±28	< 10 <sup>-10</sup>	DD						
HD 174779						HD 70702					
58 647.316	Fe I (21)	1.25	-75±12	< 10 <sup>-9</sup>	DD	58 648.008	Fe I (20)	1.26	4629±222	< 10 <sup>-10</sup>	DD
	Fe II (14)	1.20	-11±3	< 10 <sup>-10</sup>	DD		Fe II (16)	1.23	4144±153	< 10 <sup>-10</sup>	DD
	Pr III (7)	1.08	-171±25	< 10 <sup>-10</sup>	DD		Pr III (22)	1.02	4031±290	< 10 <sup>-10</sup>	DD
	Nd III (35)	1.17	-69±5	< 10 <sup>-10</sup>	DD		Nd III (8)	1.15	5788±467	< 10 <sup>-9</sup>	DD
	Eu II (3)	1.62	5±53	0.687	ND		Eu II (6)	1.54	3223±183	< 10 <sup>-10</sup>	DD
HD 176196						58 650.973	Fe I (20)	1.26	930±140	< 10 <sup>-10</sup>	DD
58 648.375	Fe I (43)	1.27	123±34	< 10 <sup>-10</sup>	DD		Fe II (16)	1.23	833±74	< 10 <sup>-10</sup>	DD
	Fe II (9)	1.13	18±20	< 10 <sup>-10</sup>	DD		Pr III (22)	1.02	1295±164	6 × 10 <sup>-7</sup>	DD
	Pr III (11)	1.08	177±47	< 10 <sup>-10</sup>	DD		Nd III (8)	1.15	1000±185	2 × 10 <sup>-5</sup>	MD
	Nd III (31)	1.17	141±37	< 10 <sup>-10</sup>	DD		Eu II (6)	1.54	2279±160	< 10 <sup>-9</sup>	DD
	Eu II (2)	1.61	129±68	8 × 10 <sup>-6</sup>	DD						
58 650.344	Fe I (43)	1.27	96±33	< 10 <sup>-10</sup>	DD						
	Fe II (9)	1.13	60±20	< 10 <sup>-10</sup>	DD						
	Pr III (11)	1.08	188±61	< 10 <sup>-10</sup>	DD						
	Nd III (31)	1.17	117±35	< 10 <sup>-10</sup>	DD						
	Eu II (2)	1.61	90±77	5 × 10 <sup>-4</sup>	MD						

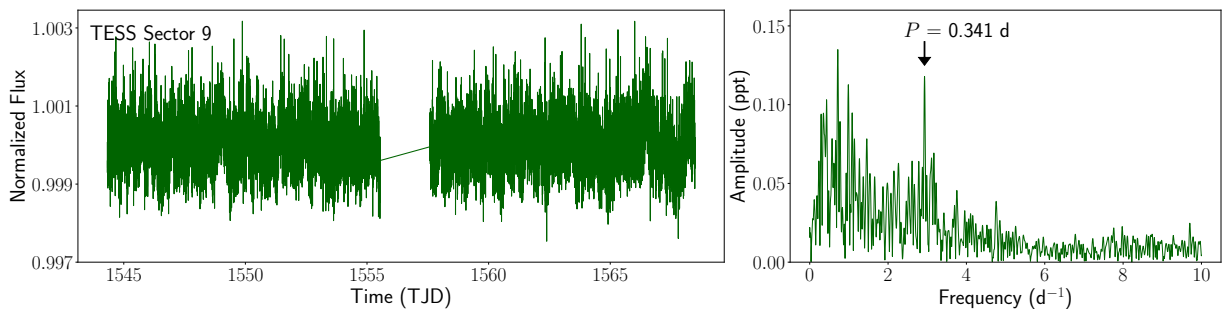


**Figure 4.** The left panel shows the TESS light curve of HD 89383 from Sector 9. The right panel shows the periodogram of this light curve. The single marginal peak is highlighted with an arrow.

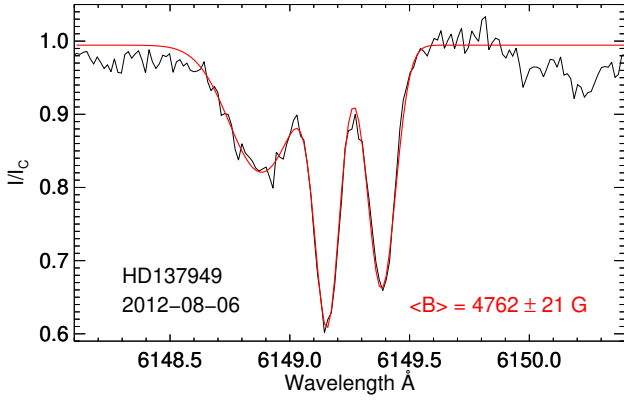


**Figure 5.** Stokes  $I$  spectra of HD 137949 in the region containing the magnetically split Fe II line at 6149.258 Å. The distance between the Zeeman subcomponents is determined using a triple Gaussian fit represented by the red solid line. It has been suggested that the leftmost component corresponds to a Sm III line.

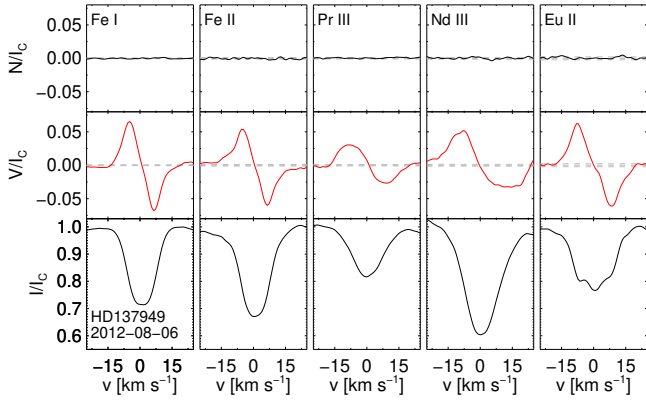


**Figure 6.** As Fig. 3, but for HD 137949.

only very poorly in the atmosphere of HD 138633. A photometric study using the STEREO satellites suggested that this star is constant or probably constant (Wraight et al. 2012). On the other hand, Romanyuk et al. (2017) report on the change of the field polarity in the measurements of the mean longitudinal magnetic field in spectra acquired in 2010 on two different nights separated by 5 days, with  $\langle B_z \rangle = 310 \pm 30 \text{ G}$  and  $\langle B_z \rangle = -290 \pm 20 \text{ G}$ .

To check the short- and long-term line profile variability of HD 138633, we compared the line profile shapes observed with HARPSpol in 2019 with those observed using UVES on 2004 March 5 and CES on 2002 January 25. In Fig. 7, we display a few line profiles observed with these spectrographs in the same spectral region as shown in Fig. 1. Some tiny changes in the line shapes between the two CES spectra separated in time by 14 minutes seem to exist, but obviously higher  $S/N$  data are needed to achieve any conclusion about any rapid spectral variability of this star.

In Fig. 8 we present the LSD Stokes  $I$ , Stokes  $V$ , and diagnostic null  $N$  profiles calculated using five different masks. Using all lines for the measurements, we obtain a positive longitudinal magnetic field on the order of 200 G, which is comparable to measurements carried out using different

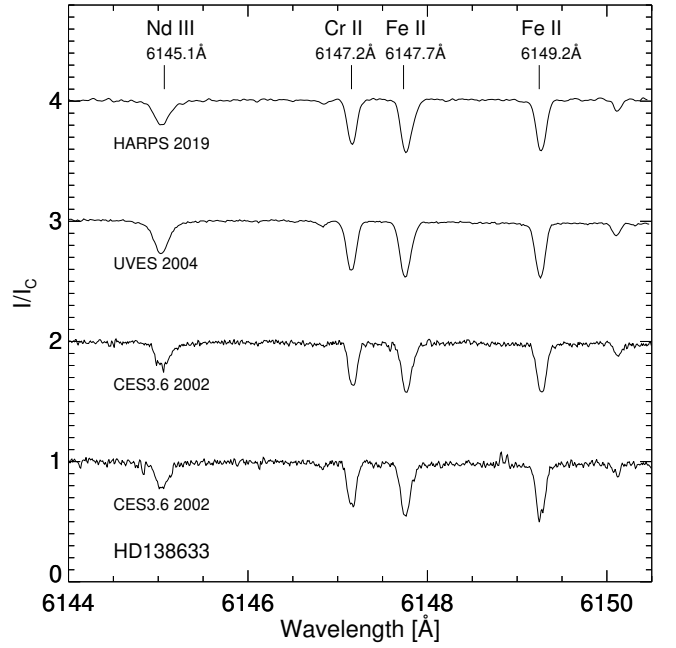


**Figure 7.** The same spectral region as shown in Fig. 1 but showing the spectra for HD 138633 obtained with different instruments between the years 2002 and 2019. The second CES spectrum was obtained 14 minutes after the first spectrum on 2002 January 25.

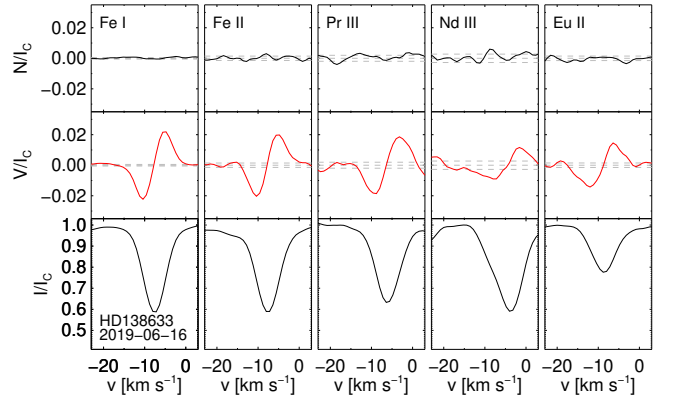


**Figure 8.** As Fig. 3 but for HD 138633.

line masks (see Tables 1–2). The strongest field,  $\langle B_z \rangle = 257 \pm 30 \text{ G}$ , is detected for the Pr III line mask. Based on the strengths of the LSD Stokes  $I$  profiles of the studied REEs, we cannot confirm the finding of Titarenko et al. (2013) that these elements are represented very poorly in the atmosphere of HD 138633.

Due to significant scattered light from both the Moon and the Earth entering Camera 1, the short-cadence TESS data of HD 138633 suffers from a data gap of approximately 10 days. Using the available photometry, we performed a DFT (see, Fig. 9) and were unable to find any significant peaks in the periodogram that could correspond to either pulsations or rotation. This suggests that this star has a long rotational period that is at least longer than the length of the TESS observations. Due to the short length and poor quality of

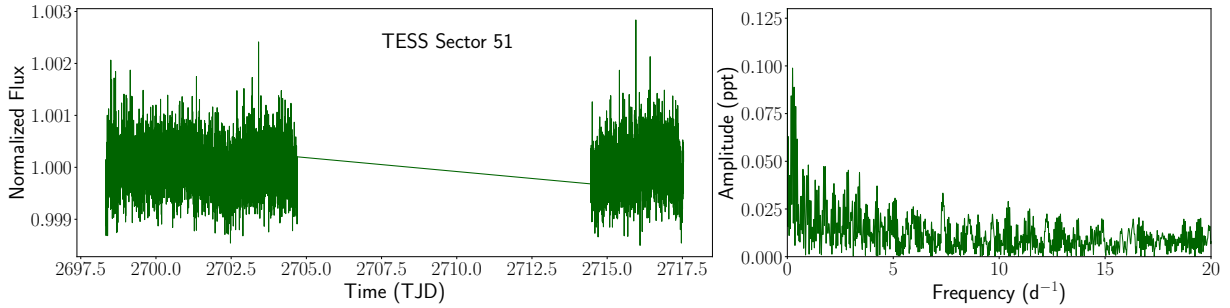


**Figure 9.** The left panel shows the TESS light curve of HD 138633 from Sector 51. The right panel shows the periodogram of this light curve. No significant peaks are detected; the higher-amplitude peaks at low frequencies are likely due to red noise and the poor quality of the data – i.e., its short length (much of the data was cut due to contamination by scattered light from the Earth and the Moon).

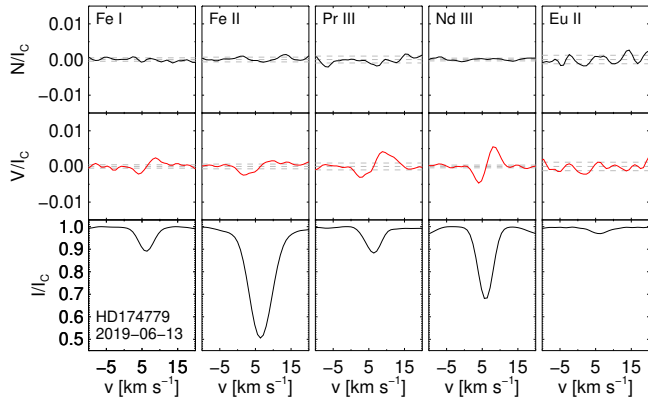


**Figure 10.** As Fig. 3, but for HD 174779.

the TESS short-cadence data, we are unable to identify any evidence for the finding of Titarenko et al. (2013) that this star belongs to the group of rapidly oscillating Ap stars and possesses a pulsation period of  $\sim 17$  min.

### 3.4 HD 174779

The star is classified as A0Si in Renson & Manfroid (2009). Catalano & Renson (1998) noted that it exhibits variability in its luminosity and/or colour, but do not report an associated period. The study of Kervella et al. (2019) indicated the presence of a companion from an analysis of proper motions in the GDR2 and Hipparcos catalogues. Magnetic field measurements have not been reported for this star in the past. Our measurements presented in Tables 1 and 2 and in Figs. 2 and 10 show that the magnetic field is very weak, with  $\langle B_z \rangle = -45 \pm 3$  G measured using all lines. It is striking that for the Pr III line mask our measurements yield a much higher field strength,  $\langle B_z \rangle = -171 \pm 25$  G, while the measurements using other masks are all below  $-75$  G. These results show that great care should be taken in the selection of line lists for the measurements of weak magnetic fields.

The analysis of the TESS observations of HD 174779 reveals two marginal peaks in the periodogram (see Fig. 11). The first corresponds to a period of  $3.7933 \pm 0.0003$  d with S/N of 4.11. The second, higher-frequency peak with a similar S/N corresponds to the period of  $1.11473 \pm 0.0001$  d. We avoid any physical interpretation of these two peaks due to

their marginal significance, and note that there is no clear, salient evidence of rotation from the light curve.

### 3.5 HD 176196

This star is classified as B9EuCr in Renson & Manfroid (2009). The study of Kervella et al. (2019) indicated the presence of a companion from an analysis of proper motions in the GDR2 and Hipparcos catalogues. First detections of the mean longitudinal magnetic field,  $\langle B_z \rangle = 258 \pm 69$  G and  $\langle B_z \rangle = 174 \pm 58$  G, were reported by Hubrig et al. (2006) using low resolution spectropolarimetry with the FORS 1 instrument installed at the ESO VLT.

Our measurements, separated by two nights, are presented in Tables 1 and 2 and in Figs. 2 and 12 and show almost identical, rather low, mean longitudinal field strengths on the order of 100–120 G. For the measurements using the Pr III line mask, the field strength reaches 180–190 G. Given the small change in the field strength since the first observations by Hubrig et al. (2006), it is very likely that the rotation period of HD 176196 is quite long.

### 3.6 HD 189832

Not much is known for this star. It is classified as A6SrCrEu in Renson & Manfroid (2009). The study of Kervella et al. (2019) indicated the presence of a companion from an analysis of proper motions in the GDR2 and Hipparcos catalogues. A rotational period  $P_{\text{rot}}$  of 18.89 d was mentioned in Manfroid & Mathys (1985), who used ground-based photometry to arrive at this value. Magnetic field measurements have not been reported for this star in the past. Similar to HD 176196, our measurements for this star, displayed in Tables 1 and 2 and in Figs. 2 and 13, show the presence of a positive weak magnetic field, with a somewhat stronger field,  $\langle B_z \rangle = 184 \pm 21$  G, measured using the Pr III line mask.

### 3.7 HD 203932

This star is classified as A5SrEu in Renson & Manfroid (2009). It is a roAp star (Kurtz 1984), with a pulsation period of about 6.2 min. Holdsworth et al. (2021) reported a rotational period of 6.44 d, based on TESS data. Mathys & Hubrig (1997) were unable to identify the presence of a magnetic field. Later on, Hubrig et al. (2004b) reported



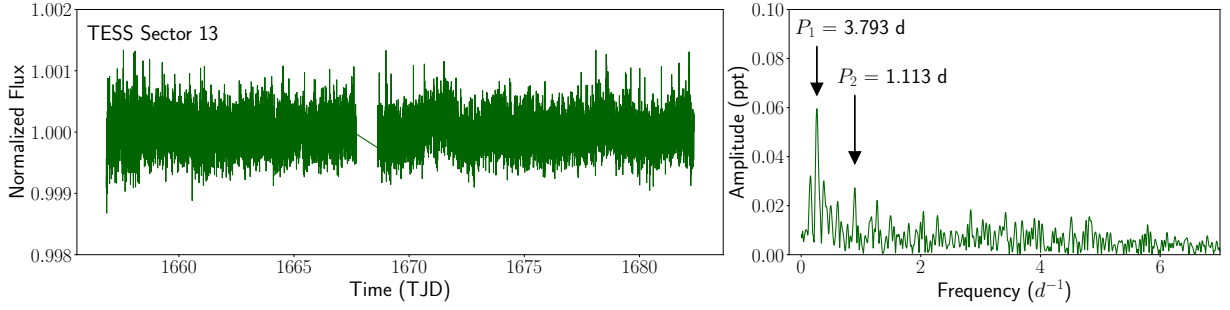


**Figure 11.** TESS light curve and periodogram for HD 174779 showing two peaks – one marginal (S/N of  $\sim 4$ ) low-frequency peak and another, higher-frequency peak with a similar S/N.

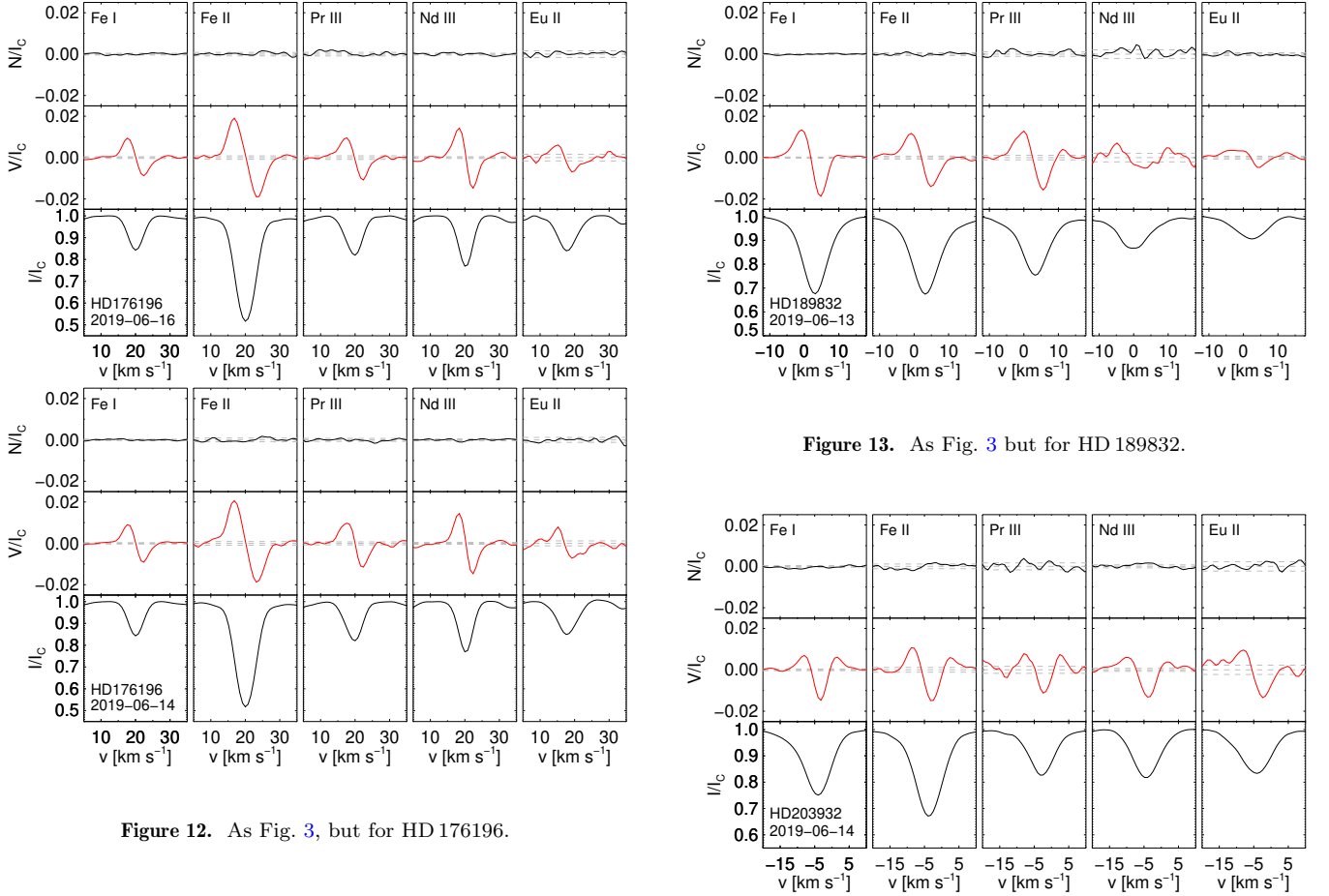


**Figure 13.** As Fig. 3 but for HD 189832.

**Figure 12.** As Fig. 3, but for HD 176196.

$\langle B_z \rangle = -267 \pm 72$  G measured in low-resolution FORS 1 polarimetric spectra acquired in 2002. Our analysis, shown in Tables 1 and 2 and in Figs. 2 and 14, yields the lowest mean longitudinal field strength when all lines are used in the measurement, but the field strength is as high as 150 G in the measurements using only the Eu II line mask. Notably, the shape of the calculated Zeeman features in Figs. 2 and 14 corresponds to a typical crossover profile, which results from the correlation between the Zeeman effect and the rotation-induced Doppler effect across the stellar surface.

### 3.8 HD 217522

This star is classified as A5SrEuCr in Renson & Manfroid (2009). It is a rapidly pulsating star with a pulsation pe-

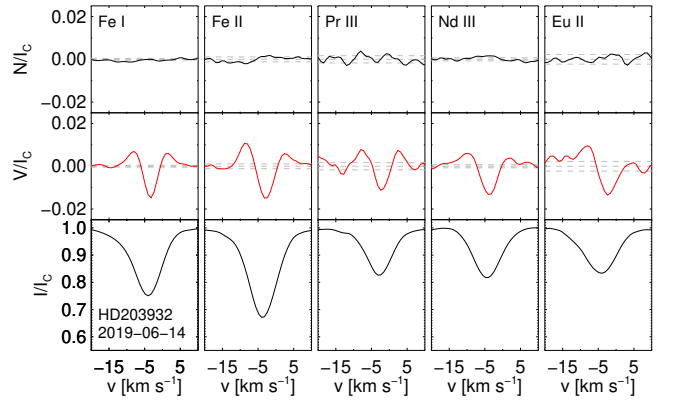


**Figure 14.** As Fig. 3 but for HD 203932.

riod of about 13.7 min (Medupe et al. 2015). Hubrig et al. (2002) showed that HD 217522 is very similar to Przybylski's star (HD 101065), which exhibits the most complex spectra known, with numerous lines of lanthanides and also rotates extremely slowly, with a probable  $P_{\text{rot}}$  of about 188 yr (Hubrig et al. 2018). The study of Kervella et al. (2019) indicated the presence of a companion from an analysis of proper motions in the GDR2 and Hipparcos catalogues, but no companion candidate was detected using diffraction-limited near-infrared imaging with NAOS-CONICA at the VLT by Schöller et al. (2012).

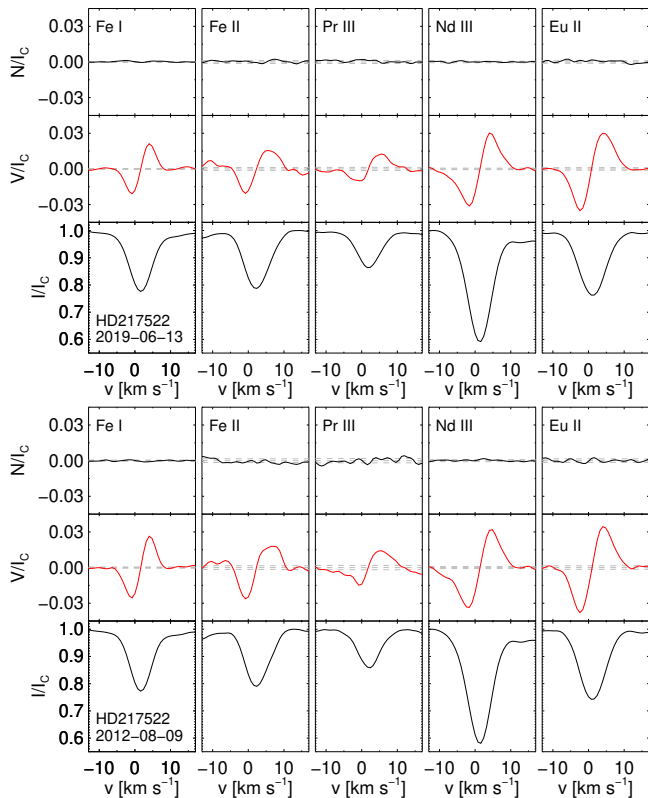


**Figure 15.** As Fig. 3, but for HD 217522.

The first detection of a magnetic field of about  $-400$  G was reported by [Mathys & Hubrig \(1997\)](#) using the ESO Cassegrain Echelle Spectrograph (CASPEC), fed by the ESO 3.6 m telescope, for observations acquired in 1992. One additional observation was obtained in 1997 with  $\langle B_z \rangle = -559 \pm 63$  G ([Hubrig et al. 2002](#)). Later, [Hubrig et al. \(2004b\)](#) reported  $\langle B_z \rangle = -725 \pm 88$  G using low-resolution spectropolarimetry with FORS 1. No variability of the field strength over the pulsation cycle was detected by [Hubrig et al. \(2004a\)](#) using a FORS 1 spectropolarimetric time series.

Our analysis presented in Tables 1 and 2 and in Figs. 2 and 15 is based on two HARPSpol observations, one from 2012 August and the second one from 2019 June. A comparison of the measurements indicates that the field in the measurements using all lines has slightly decreased from  $\langle B_z \rangle = -401 \pm 6$  G to  $\langle B_z \rangle = -323 \pm 6$  G. Assuming that the maximum field strength was reached in the year 2004, the expected rotation period should be at least of the order of a few tens of years. The strongest field strength was measured using the Pr III line mask, reaching  $\langle B_z \rangle = -552 \pm 59$  G in the observations acquired in 2012.

### 3.9 HD 70702

This star is classified as B9 EuCrSr in [Renson & Manfroid \(2009\)](#) and was used in our observations as a standard star. It possesses an extremely strong magnetic field with a mean field modulus of the order of 14–15 kG. Because of the strength of this field, numerous lines in the spectra of HD 70702 appear resolved into their magnetically split components ([Elkin,](#)

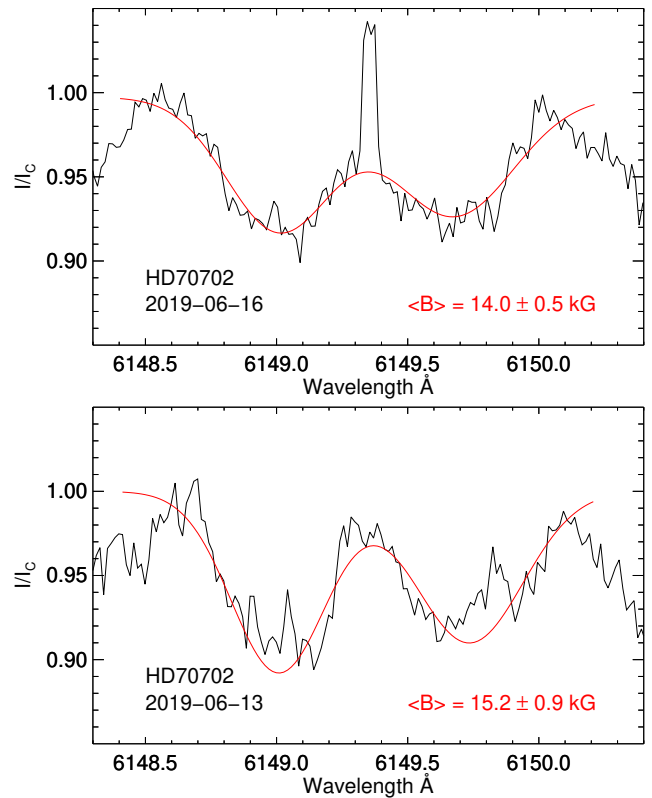


**Figure 16.** Stokes  $I$  spectra of HD 70702 in the region of the magnetically split Fe II line at  $6149.258$  Å observed at two different epochs. The line profiles are fitted by two Gaussian components represented by the red solid lines. The spectrum in the upper panel is affected by a cosmic ray appearing between the resolved components (see also the spectra for this star in Fig. 1).

[Kurtz & Nitschelm 2012](#)). Both of our HARPS spectra are rather noisy and, in addition, the precision of the measurements is limited by the distortion of the lines as a result of the combination of the Zeeman effect and the rotational Doppler effect. The measurements of the mean magnetic field modulus,  $\langle B \rangle = 15.2 \pm 0.9$  kG (from a spectrum obtained on 2019 July 13) and  $\langle B \rangle = 14.0 \pm 0.5$  kG (from a spectrum obtained on 2019 July 16), are presented in Fig. 16. They are in good agreement with the previously published value of 15 kG in [Elkin, Kurtz & Nitschelm \(2012\)](#). In Fig. 17, we present the LSD Stokes  $I$ , Stokes  $V$ , and diagnostic null  $N$  profiles calculated for both observing epochs using five different masks. The strong variability of HD 70702 is obvious and is clearly reflected in the measurement results presented in Tables 1 and 2, as well as in the distinct changes of the amplitude of the Stokes  $V$  profiles between both epochs. The strongest mean longitudinal magnetic field is detected using the Nd III line mask in the observations from the first epoch, suggesting that this element, in comparison to other elements, is concentrated in a region of the surface located closer to the magnetic pole.

In the DFT for this star, we combined the data from Sectors 8 and 9 to find three significant periods. Contamination from other stars is likely minimal, since the CROWDSAP parameter suggests that only 1.5% of the flux in the optimal aperture does not belong to HD 70702. We observe a strong

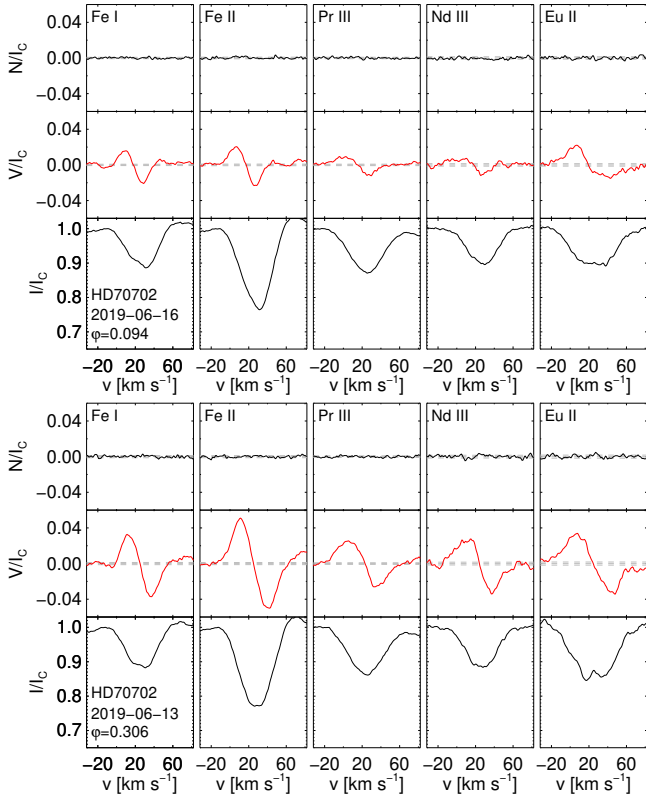


**Figure 17.** As Fig. 3, but for HD 70702. Since the rotation period is known from TESS observations, we also indicate the corresponding rotation phases.

rotational modulation with  $P_{\text{rot}} = 3.7601 \pm 0.0007$  d, as well as a short-period modulation – perhaps due to pulsation – at  $P_{\text{puls}} = 0.39019 \pm 0.00001$  d. The other significant peak, at  $P = 1.8782 \pm 0.0002$  d, has a lower  $S/N$  than the others ( $\sim 5$ ), but still meets our significance criterion. This peak can be identified as a harmonic of  $P_{\text{rot}}$ , given that it is exactly twice the frequency (to within the uncertainty of the data) of the lower-frequency peak. Using the same argument, the small peak visible near  $\nu = 5 \text{ d}^{-1}$  is almost certainly a harmonic of  $P_{\text{puls}}$ . The light curve and Fourier transform for HD 70702 are shown in Fig. 18.

Since the TESS data show a clear rotation period, we can calculate the phases of our HARPS observations. Using as initial epoch  $T_0$  the value TJD 1564.13520327 (=JD 2458564.13520327), which corresponds to the time of minimum light, we calculate  $\varphi = 0.306$  for the first observation and  $\varphi = 0.094$  for the second observation. Since this star has a rather short rotation period and possesses an extremely strong magnetic field, it is an excellent candidate for future spectropolarimetric monitoring to map its magnetic field and chemical spots using Zeeman Doppler Imaging.

#### 4 DISCUSSION AND CONCLUSIONS

Among the three sharp-lined stars not previously studied for the presence of a magnetic field (HD 89393, HD 174779, and HD 189832), the weakest mean longitudinal magnetic field,  $\langle B_z \rangle = -45 \pm 3$  G was detected in HD 174779 in the LSD

measurements using all lines, i.e. based on the line mask combining the five individual line masks. The magnetic field measurements of HD 189832 yielded a field strength of 140 G, whereas the field strength for HD 89393 was 300 G. Considering the field measurements using the five line masks separately, the strongest magnetic field was always detected for a line mask corresponding to one of the REEs: in the Eu II lines for HD 89393 and in the Pr III lines for HD 174779 and HD 189832. TESS observations of HD 89393 and HD 174779 revealed only the presence of marginal peaks at low  $S/N$ , indicating that the rotation periods of these stars are likely long. HD 189832 was reported to have a  $P_{\text{rot}} = 18.89$  d from ground-based photometry in Manfroid & Mathys (1985).

The presence of weak magnetic fields in the sharp-lined stars HD 138633, HD 176196, HD 203932, and HD 217522 was already discussed in previous studies, but the detections were, in most cases, based on low-resolution spectropolarimetric observations. The weakest mean longitudinal magnetic field,  $\langle B_z \rangle = 21 \pm 4$  G, was detected in HD 203932 using all lines for the measurements. Field strengths of the order of 120 G and 200 G were measured for HD 176196 and HD 138633, respectively. The mean longitudinal magnetic field of HD 217522 decreased from  $-400$  G to  $-323$  G over the seven years from 2012 to 2019. As for the field measurements using five line masks separately, similar to the three above discussed sharp-lined stars lacking previous magnetic field determinations, the strongest magnetic field was always detected in a line list corresponding to one of the REEs, in Pr III lines for three stars and in Eu II lines for HD 203932. These results clearly show that the most promising way to detect weak magnetic fields in sharp-lined Ap stars is to apply the LSD technique to a line mask belonging to REEs. Our finding that stronger fields are detected using REE line masks is probably explained by the location of surface REE patches in the vicinity of the magnetic poles.

TESS observations show a short  $P_{\text{rot}}$  of 6.44 d for HD 203932, which exhibits in the polarimetric spectrum a Zeeman feature with a typical crossover profile. Longer rotation periods are suggested for HD 89393, HD 138633, HD 174779, HD 176196, and HD 217522, either from TESS observations or spectropolarimetric observations. A very long rotation period, on the order of tens of years, is suggested for the strongly magnetic roAp star HD 137949.

Summarising the results of our study, out of seven sharp-lined stars, two stars, HD 174779 and HD 203932, exhibit a rather weak longitudinal magnetic field. We should, however, keep in mind that the dipole strengths for these two stars are not known yet, due to the absence of their  $\langle B_z \rangle$  phase curves. The fact that the majority of the studied stars are slow rotators – apart from HD 189832 and HD 203932, all other studied sharp-lined stars have long rotation periods – is in agreement with our expectations that the inclination angles of the rotation axes of our sample stars with respect to our line of sight are randomly distributed. This is also in agreement with the previous work of Hubrig, North & Schöller (2007). On the other hand, the absence of rotational variability can also be expected if the magnetic obliquity  $\beta$  with respect to the rotation axis is very small (e.g. Mathys, Kurtz & Holdsworth 2020). Interestingly, the study by Hubrig, North & Schöller (2007) on the evolution of magnetic fields in stars across the upper main sequence using a sample of 90 Ap and Bp stars with accurate Hipparcos parallaxes and definitely determined

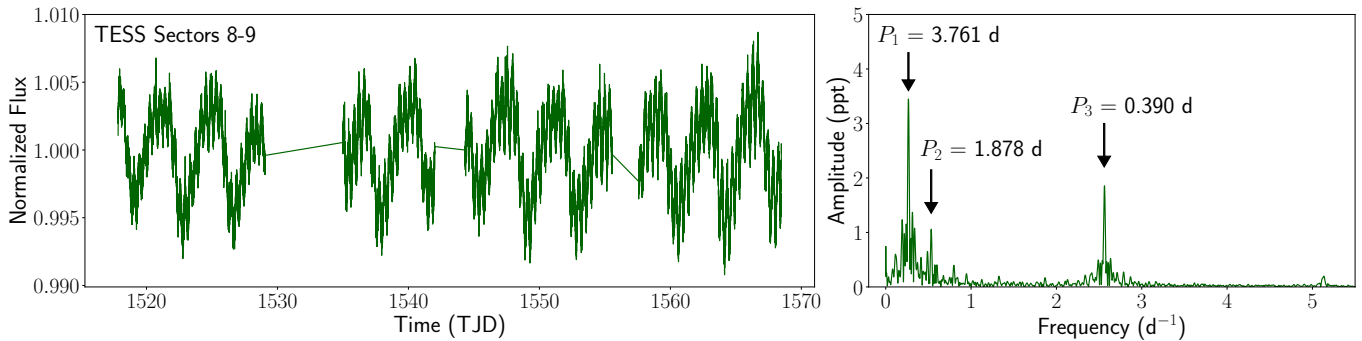


**Figure 18.** The left panel shows the TESS light curve of HD 70702 from Sectors 8 and 9. The right panel shows the periodogram of this light curve, with the three most prominent periods marked.  $P_1$  is the rotation period, and  $P_3$  is likely a pulsation period. Both periods are clearly visible in the light curve.  $P_2$  represents the first harmonic of  $P_1$ .

longitudinal magnetic field phase curves revealed that the angle  $\beta$  is smaller than  $20^\circ$  in slower rotating stars.

The rotation periods of Ap stars span up to five or six orders of magnitude (e.g. Mathys 2020a), but no evidence was previously found for any loss of angular momentum during the main-sequence lifetime (e.g. Hubrig, North & Schöller 2007). Mathys (2020b) denoted all Ap and Bp stars with rotation periods longer than 50 d as super-slowly rotating Ap (ssrAp) stars and presented accurate periods for 33 such targets, with the 29 yr period of HD 50169 being the longest of them (Mathys et al. 2019). A rotation period of about 35462.5 d ( $\sim 97$  yr) was suggested by Bychov, Bychova & Madej (2016) for the Ap star  $\gamma$  Equ (=HD 201601), and of about 188 yr for Przybylski’s star (=HD 101065) by Hubrig et al. (2018). It was also suggested that weak-field Ap stars may potentially represent a significant fraction of the group of very slowly rotating stars, with rotation periods reaching several hundred years (Mathys 2020a). An explanation for the extremely slow rotation of a fraction of Ap stars is currently missing, although a first theoretical attempt to understand this phenomenon was recently presented by Kitchatinov, Potravnov & Nepomnyashchikh (2020), who suggested a possible scenario in terms of a longitudinal drift of the unstable disturbances of a kink-type (Taylor) instability of the stellar internal magnetic field.

Our studied sample of sharp-lined Ap stars is rather small and does not allow us to decide whether a critical value for the stability of a large-scale magnetic field indeed exists, or if previous observations are incomplete, insofar as they are missing a sizeable population of chemically peculiar sharp-lined stars without any magnetic or Doppler line broadening. Therefore, additional systematic, multi-epoch  $\langle B_z \rangle$  determinations for the known Ap and Bp stars with sharp unresolved spectral lines are needed to characterise the distribution of the slowly rotating Ap stars, both in terms of their magnetic field strengths and rotation periods, in order to provide essential clues for the theoretical understanding of the formation and evolution of these stars.

## ACKNOWLEDGEMENTS

We thank the anonymous referee for their helpful comments. We also thank Gautier Mathys for the discussion on sev-

eral stars in our sample. Based on observations made with ESO Telescopes at the La Silla Paranal Observatory under programme IDs 68.D-0445, 072.D-0138, 089.D-0383, and 0103.C-0240. This paper includes data collected by the TESS mission. Funding for the TESS mission is provided by the NASA Science Mission Directorate. Resources supporting this work were provided by the NASA High-End Computing (HEC) Program through the NASA Advanced Supercomputing (NAS) Division at Ames Research Center to produce the SPOC data products. This work has made use of the VALD, operated at Uppsala University, the Institute of Astronomy RAS in Moscow, and the University of Vienna.

## DATA AVAILABILITY

The data obtained with ESO facilities are available in the ESO Archive at <http://archive.eso.org/> and can be found with the instrument and object name.

TESS light curves are publicly available through the Mikulski Archive for Space Telescopes (<https://mast.stsci.edu/portal/Mashup/Clients/Mast/Portal.html>).

## REFERENCES

- Alecian E., Tkachenko A., Neiner C., Folsom C. P., Leroy B., 2016, *A&A*, 589, A47
- Alecian G., Stift M. J., 2019, *MNRAS*, 482, 4519
- Aurière M., et al., 2007, *A&A*, 475, 1053
- Babcock H. W., 1958, *ApJS*, 3, 141
- Borucki W., et al., 2009, in Pont F., Sasselov D., Holman M. J., eds, *IAU Symposium Vol. 253*, p. 289
- Bychkov V. D., Bychkova L. V., Madej J., 2016, *MNRAS*, 455, 2567
- Catalano F. A., Renson P., 1998, *A&AS*, 127, 421
- Cunha M. S., et al., 2019, *MNRAS*, 487, 3523
- Donati J.-F., Semel M., del Toro Iniesta J. C., 1990, *A&A*, 233, L17
- Donati J.-F., Semel M., Rees D. E., 1992, *A&A*, 265, 669
- Donati J.-F., Semel M., Carter B. D., Rees D. E., Collier Cameron A., 1997, *MNRAS*, 291, 658
- Donati J.-F., et al., 2006, *MNRAS*, 370, 629
- Elkin V. G., Kurtz D. W., Nitschelm C., 2012, *MNRAS*, 420, 2727
- Fossati L., et al., 2015, *A&A*, 574, A20
- Gaia Collaboration, et al., 2018, *A&A*, 616, A1



- Giarrusso M., Cecconi M., Cosentino R., Munari M., Ghedina A., Ambrosino F., Boschini W., Leone F., 2022, *MNRAS*, 514, 3485
- Grunhut J. H., et al., 2017, *MNRAS*, 465, 243
- Holdsworth D. L., Cunha M. S., Shibahashi H., Kurtz D. W., Bowman D. M., 2018, *MNRAS*, 480, 2976
- Holdsworth D. L., et al., 2021, *MNRAS*, 506, 1073
- Howell S. B., et al., 2014, *PASP*, 126, 398
- Hubrig S., Schöller M., 2021, “Magnetic Fields in O, B, and A Stars”, ISBN: 978-0-7503-2390-1, IOP Publishing, Bristol/Tokyo
- Hubrig S., Cowley C. R., Bagnulo S., Mathys G., Ritter A., Wahlgren G. M., 2002, in Tout C. A., van Hamme W., eds, *ASP Conf. Ser.*, 279, Exotic Stars as Challenges to Evolution, p. 365
- Hubrig S., Kurtz D. W., Bagnulo S., Szeifert T., Schöller M., Mathys G., Dziembowski W. A., 2004a, *A&A*, 415, 661
- Hubrig S., Szeifert T., Schöller M., Mathys G., Kurtz D. W., 2004b, *A&A*, 415, 685
- Hubrig S., North P., Schöller M., Mathys G., 2006, *Astron. Nachr.*, 327, 289
- Hubrig S., North P., Schöller M., 2007, *Astron. Nachr.*, 328, 475
- Hubrig S., Ilyin I., Schöller M., Lo Curto G., 2013, *Astron. Nachr.*, 334, 1093
- Hubrig S., Järvinen S. P., Madej J., Bychkov V. D., Ilyin I., Schöller M., Bychkova L. V., 2018, *MNRAS*, 477, 3791
- Järvinen S. P., Hubrig S., Mathys G., Khalack V., Ilyin I., Adigozalade H., 2020, *MNRAS*, 499, 2734
- Jenkins J. M., et al., 2016, in Chiozzi G., Guzman J. C., eds, *Proc. SPIE Conf. Ser. Vol. 9913, Software and Cyberinfrastructure for Astronomy IV*. SPIE, Bellingham, p. E3
- Jermyn A. S., Cantiello M., 2020, *ApJ*, 900, 113
- Kitchatinov L. L., Potravnov I. S., Nepomnyashchikh A. A., 2020, *A&A*, 638, L9
- Kervella P., Arenou F., Mignard F., Thévenin F., 2019, *A&A*, 623, A72
- Kupka F., Dubernet M.-L., VAMDC Collaboration, 2011, *BaltA*, 20, 503
- Kurtz D. W., 1982, *MNRAS*, 200, 807
- Kurtz D. W., 1984, *MNRAS*, 209, 841
- Kurtz D. W., 1985, *MNRAS*, 213, 773
- van Leeuwen F., 2007, *A&A*, 474, 653
- Manfroid J., Mathys G., 1985, *A&AS*, 59, 429
- Mathys G., 2018, *A&A*, 601, 14
- Mathys G., 2020a, in Neiner C., Weiss W. W., Baade D., Griffin R. E., Lovekin C. C., Moffat A. F. J., eds, *Proc. of the conference “Stars and their Variability Observed from Space”*, p. 131
- Mathys G., 2020b, in Wade G., Alecian E., Bohlender D., Sigut A., eds, *Proc. of the Polish Astronomical Society*, Vol. 11. ISBN: 978-83-950430-9-3, p. 35
- Mathys G., Hubrig S., 1997, *A&AS*, 124, 475
- Mathys G., Romanyuk I. I., Hubrig S., Kudryavtsev D. O., Landstreet J. D., Schöller M., Semenko E. A., Yakunin I. A., 2019, *A&A*, 624, A32
- Mathys G., Kurtz D. W., Holdsworth D. L., 2020, *A&A*, 639, A31
- Mathys G., Kurtz D. W., Holdsworth D. L., 2022, *A&A*, 660, A70
- Medupe R., Kurtz D. W., Elkin V. G., Mguda Z., Mathys G., 2015, *MNRAS*, 446, 1347
- Renson P., Manfroid J., 2009, *A&A*, 498, 961
- Ricker G. R., et al., 2015, *Journal of Astronomical Telescopes, Instruments, and Systems*, Vol. 1, id. 014003
- Romanyuk I. I., Semenko E. A., Kudryavtsev D. O., Moiseeva A. V., Yakunin I. A., 2017, *Astrophysical Bulletin*, 72, 391
- Schöller M., Correia S., Hubrig S., Kurtz D. W., 2012, *A&A*, 545, 38
- Schöller M., et al., 2017, *A&A*, 599, A66
- Snik F., Jeffers S., Keller C., Piskunov N., Kochukhov O., Valenti J., Johns-Krull C., 2008, in McLean I. S., Casali M. M., eds, *Proc. SPIE Conf. Ser. Vol. 7014, Ground-based and Airborne Instrumentation for Astronomy II*. SPIE, Bellingham, p. E22
- Titarenko A. P., Ryabchikova T. A., Kochukhov O. P., Tsybal V. V., 2013, *Astronomy Letters*, 39, 347
- Wraight K. T., Fossati L., Netopil M., Paunzen E., Rode-Paunzen M., Bewsher D., Norton A. J., White G. J., 2012, *MNRAS*, 420, 757